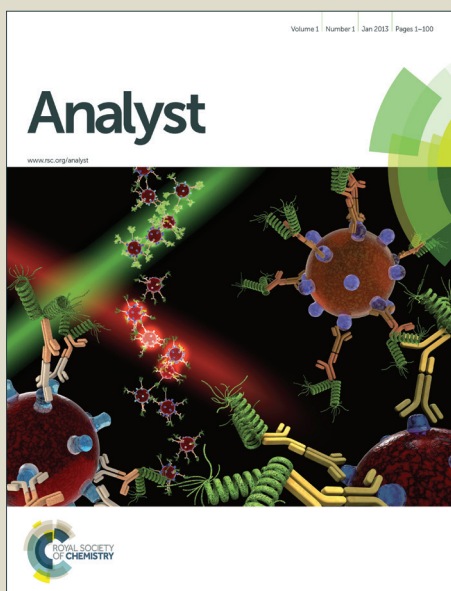


# Analyst

Accepted Manuscript



This is an *Accepted Manuscript*, which has been through the Royal Society of Chemistry peer review process and has been accepted for publication.

*Accepted Manuscripts* are published online shortly after acceptance, before technical editing, formatting and proof reading. Using this free service, authors can make their results available to the community, in citable form, before we publish the edited article. We will replace this *Accepted Manuscript* with the edited and formatted *Advance Article* as soon as it is available.

You can find more information about *Accepted Manuscripts* in the [Information for Authors](#).

Please note that technical editing may introduce minor changes to the text and/or graphics, which may alter content. The journal's standard [Terms & Conditions](#) and the [Ethical guidelines](#) still apply. In no event shall the Royal Society of Chemistry be held responsible for any errors or omissions in this *Accepted Manuscript* or any consequences arising from the use of any information it contains.

## Biochemical changes of the endothelium in the murine model of NO-deficient hypertension

Cite this: DOI: 10.1039/x0xx00000x

M. Z. Pacia<sup>a,b</sup>, L. Mateuszuk<sup>b</sup>, S. Chlopicki<sup>b,c</sup>, M. Baranska<sup>a,b</sup>, A. Kaczor<sup>a,b,\*</sup>

Received 00th January 2012,  
Accepted 00th January 2012

DOI: 10.1039/x0xx00000x

www.rsc.org/

The main spectral differences between the biochemical composition of the vascular endothelium of control, hypertensive NO-deficient, and NO-deficient mice supplemented with nitrate were studied by the use of Raman microimaging. A significantly different Raman signature of the endothelium in these three groups in the 1200-1400  $\text{cm}^{-1}$  region was assigned to the  $\alpha$ -helix and  $\beta$ -sheet alterations in the protein secondary structure upon development of hypertension. The second pronounced biochemical marker of endothelium alterations was the lipid to protein ratio. A lower intensity of the band at 2940  $\text{cm}^{-1}$  relatively to the feature at 1007  $\text{cm}^{-1}$  in the endothelium in hypertension compared to the control indicated a decrease of the lipid content relatively to proteins upon the pathology progress. The nitrate-based treatment partially reversed the effects of hypertension. The nitrate supplementation restored the lipid to protein ratio in the endothelium to the control level, while the changes in the secondary structure of proteins were irreversible upon nitrate administration.

### Introduction

Hypertension is considered to be a major risk factor for cardiovascular diseases<sup>1</sup> and is associated with vascular stiffness, alterations in vascular structure<sup>2</sup> and endothelial dysfunction. The endothelium, being the innermost layer of the vascular wall is also the important determinant of cardiovascular homeostasis. Indeed, endothelial dysfunction is a common feature of hypertension, and is associated with the loss of the balance between production of endothelium-derived relaxing factors (e.g. nitric oxide) and endothelium-derived contracting factors (e.g. angiotensin II, endothelin-1).<sup>3</sup> Among various vasodilator endothelial mediators, nitric oxide (NO) is one of the most important vasodilator that is synthesized by the endothelium from L-arginine in the reaction catalysed by endothelial nitric oxide synthase (eNOS).<sup>4</sup> Therefore, inhibition of the L-arginine/NO pathway, for example by L-NAME (N-nitro-L-arginine methyl ester), can lead to hypertension.<sup>5</sup> Besides having vasodilatory effect, NO inhibits leukocyte adhesion to the vessel wall, platelet aggregation and proliferation of vascular smooth muscle cells.<sup>6</sup> The reduced bioavailability of vascular NO, linked for example to an increased production of the reactive oxygen species in the vascular wall, results in hypertension,<sup>7</sup> that could be reversed by sodium nitrate ( $\text{NaNO}_3$ ) or nitrite ( $\text{NaNO}_2$ ) supplementation.<sup>8</sup> Hypertension has a significant effect also on the deeper layers of the vascular wall including the *tunica media*. The common feature associated with the development of hypertension is the vascular remodeling including changes in the extracellular matrix, fibrosis, and the increase in the media to lumen ratio.<sup>2</sup> The important aspect

of the extracellular matrix remodeling in hypertension is the vascular fibrosis based on the imbalance in the synthesis and degradation of elastin and collagenous components. Elastin is simultaneously synthesized and partially degraded upon development of the pathology resulting in the increased thickness of elastin fibers in the tissue.<sup>9</sup>

The major aim of our study was to identify Raman spectroscopic markers enabling distinguishing the vascular endothelium of control mice (C57BL/6J), hypertensive NO-deficient mice (treatment with L-NAME), and NO-deficient mice supplemented with sodium nitrate ( $\text{NaNO}_3$ ). The biochemical changes observed in hypertensive and nitrate-treated animals relatively to the control were visualized in the representative Raman spectra obtained by averaging of incident single spectra extracted from the endothelium area. Moreover, we checked the influence of hypertension on elastin fibers in the vascular wall. Altogether in the present work we establish the method for analysis of biochemical composition of endothelium in *ex vivo* cross section of mice aorta and identified changes induced by NO-deficiency and hypertension.

### Experimental

Three experimental groups of animals were studied: the control mice (C57BL/6J), hypertensive NO-deficient mice (8 weeks treatment with L-NAME in doses of 100 mg/kg), and NO-deficient mice supplemented with nitrate (L-NAME (100 mg/kg)/ $\text{NaNO}_3$  (1 mmol/kg)). Mice were anesthetized with ketamine (Vetoquinol) and xylazine (Bayer) solutions in doses of 80 mg and 8 mg per kg body weight, respectively. The drugs were administered intraperitoneally.

After isolation of a thoracic segment of aorta, the samples were fixed for 10 minutes in 4% buffered formalin (Merck), embedded in OCT medium (Thermo) and frozen at  $-80^{\circ}\text{C}$ . The effect of sample fixation was regarded as uniform in respect to different samples. Cross sections of  $5\ \mu\text{m}$  thickness were obtained using a microtome and mounted onto cell-Tak®-coated calcium fluoride slides. Overall, 7 control, 7 hypertensive and 3 hypertensive animals supplemented with nitrate were studied and 12, 12 and 5 Raman images, respectively, were measured. Raman imaging measurements of the aortic vessel wall were done with a Confocal Raman Imaging system WITec alpha 300 with the application of 100×air objective (Olympus, MPlan FL N, NA=0.9). The laser excitation wavelength of 532 nm, laser power of *ca.* 15 mW and integration times of 0.2 second per spectrum were used in all measurements. Images of  $140 \times 140$  pixels<sup>2</sup> and  $25 \times 25\ \mu\text{m}^2$  size were recorded. WITec Project Plus 2.10 software was employed for data preprocessing including cosmic ray removal and background correction and to perform Cluster Analysis (K-means, Manhattan distance) of obtained Raman images. In the Cluster Analysis method, Raman spectra are sorted according to their similarities. The number of clusters is determined by the operator before the data set classification. As the result it gets a certain number of clusters with different color each containing the most similar spectra from the image.<sup>10</sup>

The OPUS 7.2 program was used to calculate the integral intensity of following bands: 2940, 1108 and  $1007\ \text{cm}^{-1}$  in the regions 3030-2827, 1124-1086 and  $1023-993\ \text{cm}^{-1}$ , respectively. A straight line was drawn between the points of the two frequency limits defined. The area above this line was integrated.

The deconvolution of the Raman amide I band (in the region  $1600-1730\ \text{cm}^{-1}$ ) was performed with the commercial computer software (Origin Pro 9.1, OriginLab) with the constant baseline mode and Lorentz peak type. The number of components (6 functions) was determined based on the second derivative of band. The archived fit measured by reduced chi-squared ( $2.354\text{E-}06$  and  $2.243\text{E-}06$ ) and adjusted r-square (9.937 and 9.942) are similar for both samples from control and hypertensive mice, respectively.

An ImageJ processing program [Rasband, W. S.; U. S. National Institutes of Health: Bethesda, Maryland, USA, <http://imagej.nih.gov/ij/>, 1997-2012.] was applied to calculate the elastin fibers area.

## Results and discussion

### Univariate and Cluster Analysis of murine aorta

Although Raman spectroscopy is a convenient method to study the biochemical changes in response to the development of cardiovascular pathologies,<sup>11, 12</sup> determination of endothelium-specific alterations is not so obvious. The boundary between the *tunica intima* and *media* is not clear, and to extract the signal from the endothelium, a combination of different methods of data analysis is required.<sup>13</sup> In this study, combination of the integrative analysis with Cluster Analysis (K-means) enabled separation of the endothelium region from the *tunica media*. It was previously confirmed by immunohistochemical staining that Raman imaging enabled visualization of vessel wall compartments including endothelial nuclei.<sup>14</sup> The representative examples of Raman

integration images for three experimental groups of mice (control, hypertensive NO-deficient and hypertensive nitrate-treated) are presented in Fig. 1. The first column of Fig. 1 shows representative Raman images corresponding to the overall content of all organic compounds. The images were obtained by integration of the band due to the C–H stretching modes in the  $2800\text{--}3100\ \text{cm}^{-1}$  range. This column presents the innermost region of the vessel wall with the aorta lumen denoted by the letter L.

The images obtained by integration in the  $775\text{--}800\ \text{cm}^{-1}$  spectral region (Fig. 1, column 2), associated with the O–P–O stretching of the DNA phosphodiester bonds,<sup>15</sup> visualize the localization of the cell nuclei of both endothelial and smooth muscle cells. Distinguishing between these two types of nuclei is based on their location in the tissue. The smooth muscle cells nuclei are located inside the *tunica media* (e.g. the elongated nucleus inside the tissue; Fig. 1A2), while endothelial cell nuclei are positioned at the edge of the tissue (e.g. two circular nuclei; Fig. 1C2). The presence of cell nuclei is particularly important as a hallmark of the endothelial cells position. The third column in Fig. 1 shows the elastin fibers and was obtained by integration of the marker band at  $528\ \text{cm}^{-1}$  due to the S–S stretching vibrations.<sup>16, 17</sup> The distribution of elastin fibers, as the part of the *tunica media*, is also helpful in determining location of the endothelium, as the *tunica intima* is placed between the lumen and the internal elastic lamina.

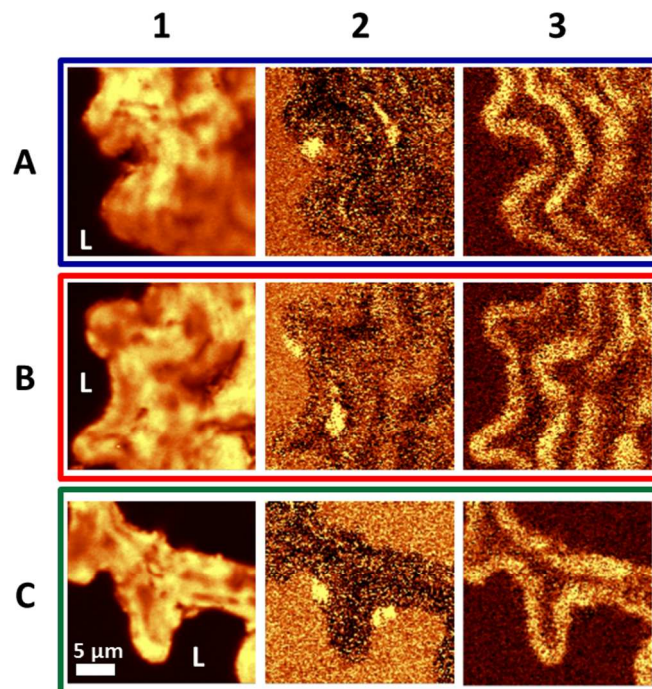


**Fig. 1.** The representative Raman images of aorta cross-sections of the control (row A), hypertensive NO-deficient (row B) and NO-deficient mice supplemented with nitrate (row C) obtained by the integration of bands due to organic specimens ( $2800\text{--}3100\ \text{cm}^{-1}$ , column 1), cell nuclei ( $775\text{--}800\ \text{cm}^{-1}$ , column 2) and elastin fibers ( $540\text{--}560\ \text{cm}^{-1}$ , column 3), respectively. “L” denotes the aorta lumen.

Results of Cluster Analysis applied to the Raman images (Fig. 2) were complementary to the results of the integrative analysis. Cluster Analysis is a statistical method used to sort data into groups according to their similarity. In Fig. 2, five separated classes with the average spectra are presented. The blue class corresponds to cell nuclei, both of the smooth muscle cells (two elongated nuclei) and an endothelial cell (one circular nucleus). Characteristic bands due to the vibrational modes typical for DNA at 788 (the O-P-O stretching vibrations) and 1582  $\text{cm}^{-1}$  (the breathing modes of DNA bases) are clearly seen in the average spectrum of this class (Fig. 2C, blue).<sup>15, 18</sup> The classes denoted by green and red are related to the elastin fibers and the endothelium, respectively. The class assigned to the endothelium is located on the edge of the tissue, near the cell nucleus. The average spectrum of the endothelium (a control mouse) differs from those of other components of the tissue mainly by the presence of two intense bands at 1128 and 1281  $\text{cm}^{-1}$  that are discussed below in the context of biochemical alterations in hypertensive NO-deficient and hypertensive nitrate-treated mice.

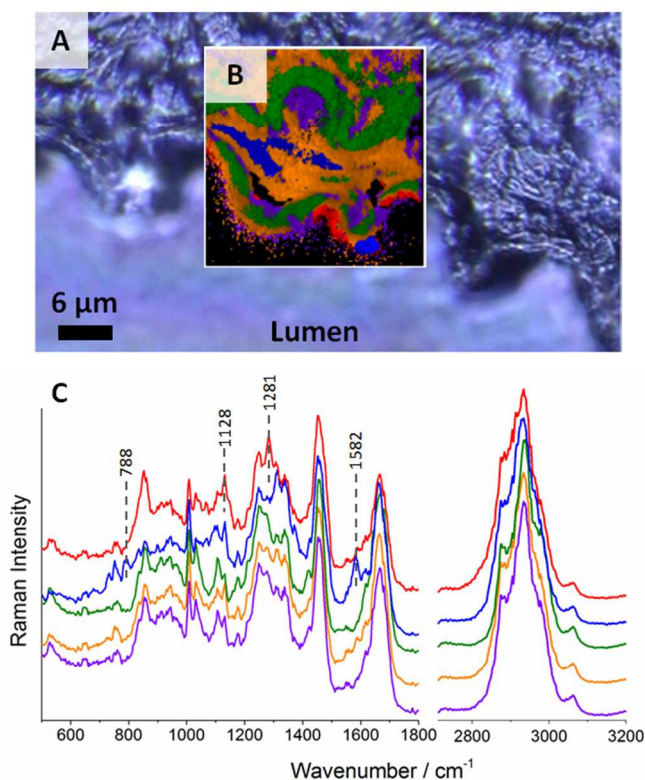


**Fig. 2.** The microphotograph of a thoracic aorta cross-section of the control mouse (A) with the cluster image (B) obtained by application of K-means (Manhattan, 5 classes) along with the average spectra of different classes (C). Red, blue and green clusters are related to the endothelium, cell nuclei and elastin fibers, respectively.

To sum up, the endothelium separation, an important step in the analysis of the cellular alterations related to hypertension, was achieved by visualization of cellular nuclei, lumen and the internal elastic lamina based on the component distribution images and Cluster Analysis.

### Structural alterations of proteins in the endothelium

In total, 12 Raman measurements were recorded both for the vessel wall of control and NO-deficient hypertensive mice and 5 for the nitrate-treated hypertensive animals. Subsequently, 30 random single spectra for control, 30 for NO-deficient hypertensive and 50 for drug-treated hypertensive mice were extracted from the endothelium region defined as described above. The respective spectra obtained by averaging of these single spectra (after normalization to the phenylalanine band at 1008  $\text{cm}^{-1}$ ) being the endothelium signature for control, hypertensive and nitrate-treated hypertensive mice are presented in Fig. 3 (fingerprint region with offset) and Fig. S1-S2 of the Supplementary Information.

The main spectral difference between the endothelium of the control and hypertensive mice is observed in the 1400-1200  $\text{cm}^{-1}$  region and is attributed to alterations in the secondary structure of proteins (Fig. 3). The secondary structure of proteins is defined by the  $\phi$  and  $\psi$  dihedral angles of the amide backbone that affect the amide I and III bands in the Raman spectra. The amide I band is attributed mainly to the amide carbonyl C=O stretching vibration, while the amide III band involves significant contribution of the C-N stretching, N-H bending, and C-C stretching modes.<sup>19</sup> The most indicative region from the point of view of the protein secondary structure is the amide III range.

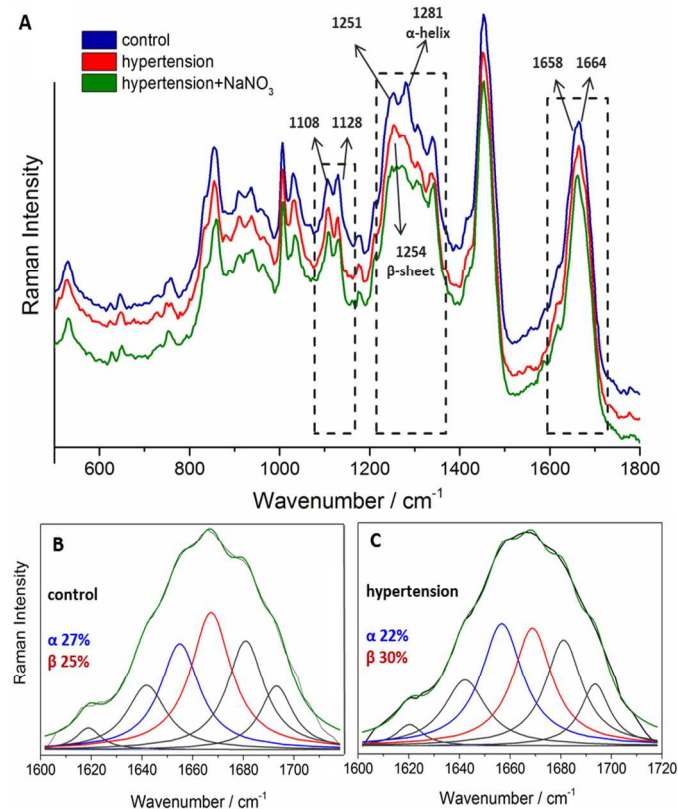


**Fig. 3.** The average spectra of control (blue: 360 spectra, 12 maps, 7 animals), NO-deficient hypertensive (red: 360 spectra, 12 maps, 7 animals) and nitrate-treated (green: 250 spectra, 5 maps, 3 animals) mice (A) taken from endothelium region. Deconvolution of the amide I band for control (B) and NO-deficient hypertensive mice (C) shows different content of the  $\alpha$  and  $\beta$  secondary structure of proteins. The blue line corresponds to the  $\alpha$ -helix (1656  $\text{cm}^{-1}$ ), the

red line to the  $\beta$ -sheet ( $1668\text{ cm}^{-1}$ ) and the green line is the sum of all the bands.

Therefore, the significant changes in the Raman spectra in the  $1200\text{-}1400\text{ cm}^{-1}$  region (Fig. 3A) are assigned to the decrease of the relative amount of the  $\alpha$ -helix structure relative to the  $\beta$ -sheet in NO-deficient hypertensive mice compared to the control. The changes of the secondary structure are observed as the decrease of the intensity of the band at  $1281\text{ cm}^{-1}$ , characteristic for the  $\alpha$ -helix protein structure, and the increase of the intensity of the counterpart at  $1254\text{ cm}^{-1}$ , assigned to the  $\beta$ -sheet. The band assignments are consistent with previous studies<sup>20-22</sup>, describing the change of the amide III band shape depending on the  $\alpha$ -helix content in the protein structure.<sup>23</sup> Obviously, protein bands in this range are partially overlapped with the bands due to lipids, however, the most intense lipid band in this region is observed at ca.  $1300\text{ cm}^{-1}$ , i.e. is considerably shifted compared to the  $\alpha$ -helix-related feature at  $1281\text{ cm}^{-1}$ .

The position of the amide I band in the  $1600\text{-}1700\text{ cm}^{-1}$  range is a consequence, *inter alia*, of the secondary structure of proteins. Here, it must be also emphasized that the band located in the  $1600\text{-}1700\text{ cm}^{-1}$  range, attributable mainly to amide I, may also include components derived from lipids, i.e. bands assigned to the C=C stretching vibrations of unsaturated triacylglycerols, cholesterol and membrane lipids.<sup>13</sup>

In the studied case (Fig. 3A), the amide I band center is observed at  $1658\text{ cm}^{-1}$  for the control, while it is shifted to  $1664\text{ cm}^{-1}$  for the endothelium of the hypertensive and hypertensive drug-treated mice. Deconvolution of the amide I band with the Lorentz functions enabled deeper insight into the alterations in the protein secondary structure for NO-deficient hypertensive mice as compared to the control (Fig. 3B-C). Although the deconvolution analysis cannot be regarded as a fully quantitative method, it allows for determination of the directions of the observed changes. Within the studied band, six counterparts are observed at  $1620$  (aromatic amino acids<sup>24, 25</sup>),  $1642$  (unordered structure<sup>26</sup>),  $1656$  ( $\alpha$ -helix<sup>24-27</sup> and lipids<sup>13</sup>),  $1668$  ( $\beta$ -sheet<sup>24-27</sup>),  $1681$  ( $\beta$ -turns<sup>25, 26</sup>) and  $1693\text{ cm}^{-1}$  (amino acids: glutamine and arginine<sup>25</sup>). For both types of samples: control and hypertension, the positions of the counterparts are the same, while the contribution of two crucial bands located at  $1656$  ( $\alpha$ -helix and lipids, blue line in Fig. 3 B-C) and  $1668\text{ cm}^{-1}$  ( $\beta$ -sheet, red line in Fig. 3 B-C) is changed. The estimated content of the  $\alpha$  and  $\beta$  secondary structures is determined as the ratio of the integral intensity of the counterpart due to the  $\alpha$  or  $\beta$  structure to the integral intensity of the amide I band.<sup>27</sup> Upon development of hypertension the relative abundance of the band at  $1656\text{ cm}^{-1}$  decreases from 27 to 22% in favour of the counterpart at  $1668\text{ cm}^{-1}$  that increases from 25 to 30%.

The relative decrease of the band at  $1656\text{ cm}^{-1}$  may be related to the parallel decrease of the  $\alpha$ -helix structure and the lipid content. The relative decrease of the  $\alpha$ -helix structure was previously discussed based on the Raman signature of the amide III band (Fig. 3A), while the changes in lipids and proteins relative content upon the development of hypertension are described in the next section. The increase of the relative intensity of the counterpart at  $1668\text{ cm}^{-1}$  is a certain sign of the  $\beta$ -sheet content growth upon pathology.

The shape of the amide III band in the spectrum of the NO-deficient nitrate treated is more similar to NO-deficient untreated mice than to the spectrum for control, indicating that the change of the protein secondary structure in hypertension may be irreversible upon nitrate treatment.

Obviously, in the biological samples such as tissues or cells all the types of secondary protein structure are possible and only the detection of changes in the relative amount of secondary structure can be possible. Generally, when the  $\alpha$ -helix structure is favoured, the displacing of the equilibrium towards the  $\beta$ -sheet is possible under the influence of factors such as heating<sup>23, 25</sup>, pH<sup>28, 29</sup>, pressure<sup>27</sup>, solvents<sup>21</sup> and lyophilisation.<sup>30, 31</sup> Furthermore, the structure conversion may also have important implications for diseases related to amyloid formation e.g. Parkinson's, where native proteins convert to  $\beta$ -sheet rich proteins.<sup>24</sup> Besides the model studies, the changes in the protein secondary structure from the  $\alpha$  helix to the  $\beta$  sheet have been also observed upon pathology development the melanoma skin cancer<sup>32</sup> or diabetes.<sup>33</sup> Additionally, during development of cardiovascular pathology, the endothelium-derived contracting factors (EDCFs) such as endothelins and angiotensin are produced in excess.<sup>3, 34</sup> Both of mentioned proteins: endothelin-1<sup>35</sup> and angiotensin II<sup>36</sup> adopt preferentially the  $\beta$ -sheet structure.

It is known that during the  $\alpha$  to  $\beta$  conversion the stiffness of the protein significantly increases.<sup>28</sup> Indeed, the increased stiffness of endothelial cells was associated with reduced bioavailability of vascular NO.<sup>37, 38</sup> The reduced activity of NO is also a common feature of endothelial dysfunction upon development of hypertension.<sup>5</sup> Up to now, the increased stiffness of NO-deficient endothelium was explained rather by the rearrangement of actin cytoskeleton.<sup>39-41</sup> Based on our results, we are tempted to speculate that the changes in the secondary structure of proteins might well be also responsible for stiffening of endothelial cells upon development of hypertension.

#### Chemical changes in the endothelium

The next important change of the endothelium in hypertension is related to the lipid to protein ratio (Fig. 4A). The overall lipid content was calculated as the ratio of the integral intensity of the band for lipids and proteins (centred at  $2940\text{ cm}^{-1}$ , assigned to the C-H stretching vibrations) to the protein marker band (at  $1007\text{ cm}^{-1}$ , assigned to the ring breathing mode of phenylalanine). It is clear that the lipid content significantly decreases in hypertension compared to the control ( $p=0.041$ , with 5% level of decision using the Tukey test in ANOVA). Moreover, the lipid to protein ratio in the endothelium of the nitrate -treated mice returns to the normal level ( $p=0.051$  for hypertension+NaNO<sub>3</sub> vs hypertension) indicating that the endothelial lipid to protein ratio can be restored to the control level upon nitrate treatment.

Additionally, changes of the relative intensity of the band at  $1108\text{ cm}^{-1}$  are observed. This band is usually assigned to the twisting vibrations of the NH<sub>2</sub> group<sup>42</sup> and aromatic ring breathing (ring with N)<sup>43</sup> vibrations in the structure of amino acids e.g. valine, arginine, tryptophan, histidine<sup>44</sup> and desmosine.<sup>16</sup> The ratio of the relative intensity of the bands at  $1108$  and  $1007\text{ cm}^{-1}$  varies in the Raman spectra of the endothelium of control, NO-deficient hypertensive and nitrate-treated mice (Fig. 4B).

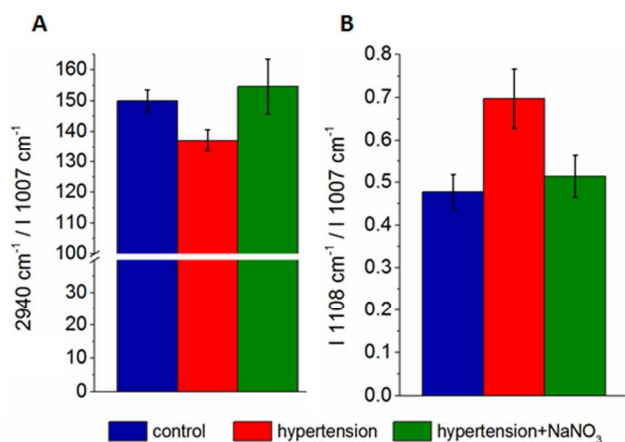


**Fig. 4.** The ratio of integral intensity of bands at 2940 to 1007  $\text{cm}^{-1}$  (A) and 1108 to 1007  $\text{cm}^{-1}$  (B) in the endothelium of the control, NO-deficient hypertensive and NO-deficient drug-treated samples.

In the spectrum of the control and nitrate-treated animals the 1108  $\text{cm}^{-1}$  band shows the considerably lower relative intensity to the 1007  $\text{cm}^{-1}$  one, while the opposite is seen in the spectrum of the endothelium of the NO-deficient hypertensive mice. The calculated p value between the control and hypertensive samples indicates statistical significance and is equal to 0.012 (with 5% level of decision using the Tukey test in ANOVA). Although the trend indicates a positive effect of treatment, no statistically significant difference between hypertensive and treated mice was observed. The ratio demonstrates the changes in the relative intensity of two bands connected with proteins. The significant increase of the band at 1108  $\text{cm}^{-1}$  upon hypertension indicates the overexpression of proteins/amino acids rich in  $\text{NH}_2$  or N in the aromatic ring.

The possible explanation of the increase of intensity of the band at 1108  $\text{cm}^{-1}$  is the increase of the content of elastin-forming amino acids. The specific amino acids in the elastin structure: desmosine and isodesmosine are rich in the  $\text{NH}_2$  groups in their structure, therefore the distinct 1108  $\text{cm}^{-1}$  band is observed in their Raman spectra.<sup>16, 17</sup> Moreover, elastin-forming amino acids can be produced by endothelial cells<sup>45, 46</sup>, what was proved by tracking the process of incorporation of  $^{14}\text{C}$ -labelled desmosine into the endothelial cells.<sup>47</sup> It could well be that the increase in the amount of elastin-forming amino acids in the endothelium is a consequence of hypertension. Indeed, upon the hypertension development, endothelial cells produce more elastin needed for remodeling of the subendothelial extracellular matrix and basic lamina (endothelial basal membrane) as a response to the increase in blood pressure.<sup>48</sup>

#### Structural alterations of elastin fibers

The effect of hypertension is not only limited to the endothelium within the *tunica intima* but is also associated with structural and mechanical abnormalities in the *tunica media*. This effect is observed in the Raman images as thickening of elastin fibers in the vascular wall of hypertensive NO-deficient and nitrate-treated mice compared to the control (Fig. 5). The details about procedure of calculation is presented in Fig. S3 of the Supplementary Information.

There are few widely recognized hallmarks of hypertension<sup>49</sup>, large artery stiffening<sup>50</sup>, extension of the extracellular matrix including elastin and collagenous fibers and the resistance artery narrowing.<sup>2</sup> Previous works carried out on hypertensive mice<sup>9, 51</sup> or rats<sup>52, 53</sup> demonstrated the alterations in the composition of the extracellular matrix during development of this pathology. Remodeling of the vascular wall implies imbalance in the synthesis and degradation of elastin and collagenous components. Upon the physiological conditions elastin turnover is constant while during pathological circumstances, elastin is synthesized and partially degrades leading to the increase in the amount of elastin fibers in the tissue.<sup>9</sup> These data are in agreement with our results. Based on Raman images of elastin fibers of control (Fig. 5A), NO-deficient hypertensive (Fig. 5B) and nitrate-treated hypertensive mice (Fig. 5C) it is possible to calculate the area of the tissue covered by elastin fibers. Upon hypertension development the effect of extension of elastin components is very significant - p value equals 0.00000618 (Fig. 5D). For the NO-deficient mice supplemented with nitrates the thickness of elastin fibers are practically unchanged compared to the NO-deficient subjects, showing that tissue remodeling in the tunica media is irreversible upon nitrate treatment.

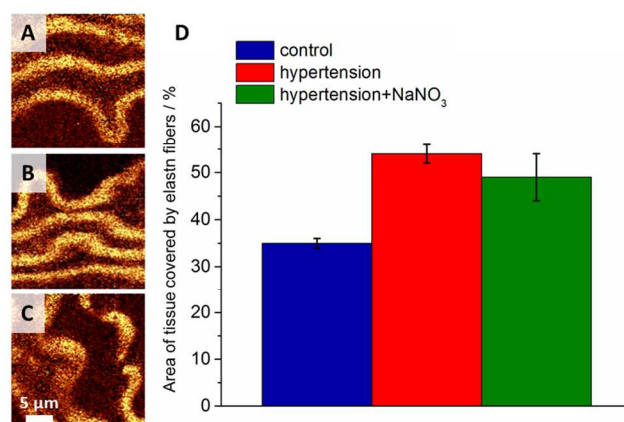


**Fig. 5.** Raman integration images of elastin fibers (integration over 540-560  $\text{cm}^{-1}$  range) in the vessel walls of control (A), NO-deficient hypertensive (B) and nitrate-treated hypertensive mice (C). Calculated tissue areas covered by elastin fibers (D).

#### Conclusions

In this study, Raman microimaging was used to study biochemical alterations in the endothelium upon hypertension development and nitrate treatment in the murine model of hypertension. The major changes in the Raman spectra of the endothelium in hypertension were observed in the profile of the amide I and III bands. These changes were related with the alterations in the secondary structure of the endothelial proteins, particularly the increase of the  $\beta$  sheet content at the expense of the  $\alpha$  helix structures and/or formation of the proteins with the high  $\beta$  sheet content. We hypothesize, that alterations of the protein secondary structure, irreversible upon nitrate treatment, represent a feature of endothelial response to

hypertension development and could contribute to the increased stiffness of the endothelium in NO-deficiency state.

Vascular remodelling was also clearly observed in the Raman images of the *tunica media* as the thickening of the elastin fibers. Also this pathological feature remained practically unchanged upon nitrate-treatment.

Other key spectroscopic markers of hypertension in the endothelium were connected with the chemical imbalance. Namely, the pathology development caused the decrease of the endothelial lipid to protein ratio and the relative increase (compared to proteins) of the content of the species manifested by the band at 1108 cm<sup>-1</sup>, possibly related with the increased production of elastin-forming amino acids (desmosine and isodesmosine) in the endothelium upon the pathology development.

An important conclusion reached in this study was related to the efficacy of nitrate supplementation. Structural changes of the vascular wall occurring upon hypertension development (changes in the secondary structure of endothelial proteins and thickening of the elastin fibers in the *tunica media*) remained treatment-resistant. On the contrary, supplementation with nitrates reversed chemical changes in the endothelium as both lipid to protein imbalance and the alterations related to the band at 1108 cm<sup>-1</sup>, possibly invoked by overproduction of desmosine and isodesmosine, were restored to the control level.

Overall, Raman microscopy enabled insight into sub-cellular changes occurring in the endothelium and the *tunica media* upon hypertension development and nitrate treatment. Accordingly, Raman spectroscopy appears as a useful tool to verify the functional status of the endothelium and to diagnose NO-deficiency of endothelium. If so, one can envisage practical application of Raman spectroscopy e.g. in the context of the intraoperative application of Raman spectroscopy to verify functional integrity of vascular graft endothelium.

## Acknowledgements

The project was supported by National Science Centre (DEC-2013/08/A/ST4/00308) and by the European Union under the European Regional Development Fund (grant coordinated by JCET-UJ, POIG.01.01.02-00-069/09).

## Notes and references

<sup>a</sup>Faculty of Chemistry, Jagiellonian University, Ingardena 3, 30-060 Krakow, Poland.

<sup>b</sup>Jagiellonian Centre for Experimental Therapeutics (JCET), Jagiellonian University, Bobrzynskiego 14, 30-348 Krakow, Poland.

<sup>c</sup>Department of Experimental Pharmacology, Jagiellonian University, Grzegorzeczka 16, 31-531 Krakow, Poland.

Electronic Supplementary Information (ESI) available: The average spectra of the endothelium of control, NO-deficient hypertensive and hypertensive treated with NaNO<sub>3</sub> mice in the fingerprint (500-1800 cm<sup>-1</sup>) and C-H (2700-3200 cm<sup>-1</sup>) regions.

1. M. Cymerys, P. Bogdanski, D. Pupek-Musialik, A. Jablęcka, J. Lacki, I. Korczowska and J. Dytfeld, *Med. Sci. Monit.*, 2012, **18**, CR330-336.
2. H. D. Intengan and E. L. Schiffrin, *Hypertension*, 2001, **38**, 581-587.

3. E. H. Tang and P. M. Vanhoutte, *Pflugers Arch., EJP*, 2010, **459**, 995-1004.
4. M. Hermann, A. Flammer and T. F. Lüscher, *J. Clin. Hypertens.*, 2006, **8**, 17-29.
5. J. A. Muldowney, S. N. Davis, D. E. Vaughan and N. J. Brown, *Hypertension*, 2004, **44**, 739-745.
6. U. Förstermann and T. Münzel, *Circulation*, 2006, **113**, 1708-1714.
7. U. Förstermann, *Pflugers Arch., EJP*, 2010, **459**, 923-939.
8. M. F. Montenegro, J. H. Amaral, L. C. Pinheiro, E. K. Sakamoto, G. C. Ferreira, R. I. Reis, D. M. Marcal, R. P. Pereira and J. E. Tanus-Santos, *Free Radic. Biol. Med.*, 2011, **51**, 144-152.
9. M. M. Steed, N. Tyagi, U. Sen, D. A. Schuschke, I. G. Joshua and S. C. Tyagi, *Am. J. Physiol.: Lung Cell. Mol. Physiol.*, 2010, **299**, L301-L311.
10. F. Bonnier, P. Knief, B. Lim, A. D. Meade, J. Dorney, K. Bhattacharya, F. M. Lyng and H. J. Byrne, *Analyst*, 2010, **135**, 3169-3177.
11. C. Krafft, L. Neudert, T. Simat and R. Salzer, *Spectrochim. Acta A Mol. Biomol. Spectrosc.*, 2005, **61**, 1529-1535.
12. M. Pilarczyk, L. Mateuszuk, A. Rygula, M. Kepczynski, S. Chlopicki, M. Baranska and A. Kaczor, *PLoS One*, 2014, **9**, DOI: 10.1371/journal.pone.0106065.
13. K. Czamara, K. Majzner, M. Z. Pacia, K. Kamila, K. Agnieszka and B. Malgorzata, *J. Raman Spectr.*, 2014, DOI:10.1002/jrs.4607.
14. M. Pilarczyk, A. Rygula, L. Mateuszuk, S. Chlopicki, M. Baranska and A. Kaczor, *Biomed. Spectrosc. Imag.*, 2013, **2**, 191-197.
15. A. Boyd, L. McManus, G. Burke and B. Meenan, *J. Mater. Sci. Mater. Med.*, 2011, **22**, 1923-1930.
16. B. G. Frushour and J. L. Koenig, *Biopolymers*, 1975, **14**, 379-391.
17. E. Green, R. Ellis and P. Winlove, *Biopolymers*, 2008, **89**, 931-940.
18. K. Majzner, A. Kaczor, N. Kachamakova-Trojanowska, A. Fedorowicz, S. Chlopicki and M. Baranska, *Analyst*, 2012, **138**, 603-610.
19. J. T. Pelton and L. R. McLean, *Anal. Biochem.*, 2000, **277**, 167-176.
20. I. Notingher, S. Verrier, H. Romanska, A. Bishop, J. Polak and L. Hench, *Spectrosc. Int. J.*, 2002, **16**, 43-51.
21. N. C. Maiti, M. M. Apetri, M. G. Zagorski, P. R. Carey and V. E. Anderson, *J. Am. Chem. Soc.*, 2004, **126**, 2399-2408.
22. Z. Chi, X. Chen, J. S. Holtz and S. A. Asher, *Biochemistry*, 1998, **37**, 2854-2864.
23. S. A. Asher, A. Ianoul, G. Mix, M. N. Boyden, A. Karnoup, M. Diem and R. Schweitzer-Stenner, *J. Am. Chem. Soc.*, 2001, **123**, 11775-11781.
24. M. M. Apetri, N. C. Maiti, M. G. Zagorski, P. R. Carey and V. E. Anderson, *J. Mol. Biol.*, 2006, **355**, 63-71.
25. A. Tfayli, O. Piot, F. Draux, F. Pitre and M. Manfait, *Biopolymers*, 2007, **87**, 261-274.
26. G. M. Kavanagh, A. H. Clark and S. B. Ross-Murphy, *Rheol. Acta*, 2002, **41**, 276-284.
27. S. Ngarize, H. Herman, A. Adams and N. Howell, *J. Agric. Food Chem.*, 2004, **52**, 6470-6477.
28. Z. Qin and M. J. Buehler, *Phys. Rev. Lett.*, 2010, **104**, 198304.
29. T. Koga, K. Taguchi, Y. Kobuke, T. Kinoshita and M. Higuchi, *Chemistry (Easton)*, 2003, **9**, 1146-1156.
30. M. van de Weert, P. I. Haris, W. E. Hennink and D. J. Crammelin, *Anal. Biochem.*, 2001, **297**, 160-169.
31. S. D. Allison, A. Dong and J. F. Carpenter, *Biophys. J.*, 1996, **71**, 2022-2032.
32. M. Gniadecka, P. A. Philipsen, S. Sigurdsson, S. Wessel, O. F. Nielsen, D. H. Christensen, J. Hercogova, K. Rossen, H. K. Thomsen and R. Gniadecki, *J. Invest. Dermatol.*, 2004, **122**, 443-449.
33. K. Majzner, T. P. Wrobel, A. Fedorowicz, S. Chlopicki and M. Baranska, *Analyst*, 2013, **138**, 7400-7410.
34. P. Sventek, J.-S. Li, K. Grove, C. F. Deschepper and E. L. Schiffrin, *Hypertension*, 1996, **27**, 49-55.
35. J. P. Huggins and J. T. Pelton, *Endothelins in biology and medicine*, CRC Press, 1996.
36. S. Fermandjian, P. Fromageot, A. M. Tistchenko, J. P. Leicknam and M. Lutz, *Eur. J. Biochem.*, 1972, **28**, 174-182.
37. K. Kusche-Vihrog, P. Jeggle and H. Oberleithner, *Pflugers Arch. - Eur. J. Physiol.*, 2014, **466**, 851-859.
38. H. Oberleithner, W. Peters, K. Kusche-Vihrog, S. Korte, H. Schillers, K. Kliche and K. Oberleithner, *Pflugers Arch. - Eur. J. Physiol.*, 2011, **462**, 519-528.
39. J. Fels, P. Jeggle, K. Kusche-Vihrog and H. Oberleithner, *PLoS One*, 2012, **7**, e41520.

- 1 40. K. Kusche-Vihrog, A. Tarjus, J. Fels and F. Jaisser, *Curr. Opin.*
- 2 *Nephrol. Hypertens.*, 2014, **23**, 143-148.
- 3 41. Y. Su, S. Edwards-Bennett, M. R. Bubb and E. R. Block, *Am. J.*
- 4 *Physiol.-Cell. Ph.*, 2003, **284**, 1542-1549.
- 5 42. J. Suh and M. Moskovits, *J. Am. Chem. Soc.*, 1986, **108**, 4711-4718.
- 6 43. M. Baia, S. Astilean and T. Iliescu, *Raman and SERS investigations of*
- 7 *pharmaceuticals*, Springer, 2008, 3540782826.
- 8 44. J. De Gelder, K. De Gussem, P. Vandenabeele and L. Moens, *J. Raman*
- 9 *Spectrosc.*, 2007, **38**, 1133-1147.
- 10 45. E. A. Jaffe, *Ann. N. Y. Acad. Sci.*, 1985, **454**, 279-291.
- 11 46. O. Tokunaga and T. Watanabe, *In Vitro Cell. Dev. Biol.*, 1987, **23**, 528-
- 12 534.
- 13 47. J. O. Cantor, M. S. Parshley, I. Mandl and G. M. Turino, in *Biology of*
- 14 *Endothelial Cells*, Springer, 1984, pp. 189-193.
- 15 48. J. W. Tobias, M. M. Bern, P. A. Netland and B. R. Zetter, *Blood*, 1987,
- 16 **69**, 1265-1268.
- 17 49. S. M. Arribas, A. Hinek and M. C. González, *Pharmacol. Ther.*, 2006,
- 18 **111**, 771-791.
- 19 50. G. M. London and J. N. Cohn, *Am. J. Hypertens.*, 2002, **15**, 754-758.
- 20 51. J. E. Wagenseil and R. P. Mecham, *J. Cardiovasc. Transl. Res.*, 2012, **5**,
- 21 264-273.
- 22 52. H. Wolinsky, *Circ. Res.*, 1971, **28**, 622-637.
- 23 53. C. Berry and S. Greenwald, *Cardiovasc. Res.*, 1976, **10**, 437-451.
- 24
- 25
- 26
- 27
- 28
- 29
- 30
- 31
- 32
- 33
- 34
- 35
- 36
- 37
- 38
- 39
- 40
- 41
- 42
- 43
- 44
- 45
- 46
- 47
- 48
- 49
- 50
- 51
- 52
- 53
- 54
- 55
- 56
- 57
- 58
- 59
- 60

## Biochemical changes of the endothelium in the murine model of NO-deficient hypertension

M. Z. Pacia, L. Mateuszuk, S. Chlopicki, M. Baranska, A. Kaczor\*

Alterations in the  $\alpha$ -helix and  $\beta$ -sheet content and lipid-to-protein ratio are most striking features of hypertension development in vascular endothelium.

